NANO LETTERS

Subscriber access provided by DALIAN INST OF CHEM PHYSICS

Letter

Photovoltaic Measurements in Single-Nanowire Silicon Solar Cells

Michael D. Kelzenberg, Daniel B. Turner-Evans, Brendan M. Kayes,
Michael A. Filler, Morgan C. Putnam, Nathan S. Lewis, and Harry A. Atwater

Nano Lett., **2008**, 8 (2), 710-714• DOI: 10.1021/nl072622p • Publication Date (Web): 13 February 2008

Downloaded from http://pubs.acs.org on February 22, 2009

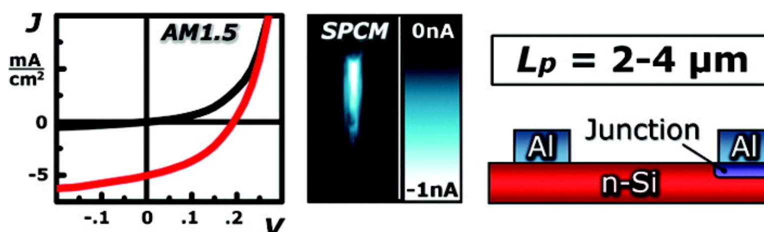

More About This Article

Additional resources and features associated with this article are available within the HTML version:

- Supporting Information
- Links to the 14 articles that cite this article, as of the time of this article download
- Access to high resolution figures
- Links to articles and content related to this article
- Copyright permission to reproduce figures and/or text from this article

View the Full Text HTML

ACS Publications
High quality. High impact.

Nano Letters is published by the American Chemical Society. 1155 Sixteenth Street N.W., Washington, DC 20036

NANO LETTERS

2008
Vol. 8, No. 2
710−714

Photovoltaic Measurements in Single-Nanowire Silicon Solar Cells

Michael D. Kelzenberg, Daniel B. Turner-Evans, Brendan M. Kayes, Michael A. Filler, Morgan C. Putnam, Nathan S. Lewis,* and Harry A. Atwater*

California Institute of Technology, Pasadena, California 91125

Received October 10, 2007

ABSTRACT

Single-nanowire solar cells were created by forming rectifying junctions in electrically contacted vapor–liquid–solid-grown Si nanowires. The nanowires had diameters in the range of 200 nm to 1.5 μm. Dark and light current–voltage measurements were made under simulated Air Mass 1.5 global illumination. Photovoltaic spectral response measurements were also performed. Scanning photocurrent microscopy indicated that the Si nanowire devices had minority carrier diffusion lengths of ∼2 μm. Assuming bulk-dominated recombination, this value corresponds to a minimum carrier lifetime of ∼15 ns, or assuming surface-dominated recombination, to a maximum surface recombination velocity of approximately 1350 cm s^{-1}. The methods described herein comprise a valuable platform for measuring the properties of semiconductor nanowires, and are expected to be instrumental when designing an efficient macroscopic solar cell based on arrays of such nanostructures.

Semiconductor nanowires offer exciting possibilities as components of solar cells and have already found applications as antireflective layers[1−3] and as active elements in organic,[4] dye-sensitized,[5,6] quantum-dot sensitized,[7] liquid-junction,[8,9] and inorganic solid-state[2] devices. Our efforts are in pursuit of a solid-state Si nanowire array solar cell in which each wire has a p-n junction in the radial direction. By orthogonalizing the direction of light absorption and carrier collection, radial junctions can enable efficient carrier collection in optically thick nanowire arrays, even when minority carrier diffusion lengths are shorter than the optical absorption length.[10] This design has the potential to enable energy-conversion efficiencies near that of wafer-based crystalline Si solar cells but at costs competitive with thin-film technologies. Previous work by our group has shown that macroscopic Si wire arrays (>1 cm^2 in area) suitable for photovoltaic applications can be grown rapidly by the vapor−liquid−solid (VLS) process using inexpensive, earth-abundant growth catalysts such as Cu.[11] To obtain optimal energy-conversion efficiencies for solar cells based on nanowire arrays, an understanding of individual nanowire photovoltaic performance is necessary. While others have determined the minority carrier diffusion length in single-nanowire CdS photovoltaic devices,[12,13] to our knowledge no such measurement has been reported for single-nanowire Si solar cells. Therefore, we present herein the fabrication of a single-nanowire Si solar cell, along with methods to measure its minority carrier diffusion length, spectral response characteristics, and the dark and light current−voltage ($I-V$) properties under simulated Air Mass 1.5 global (AM 1.5G) illumination. These methods provide a simple and useful platform for gaining insight into nanowire charge transport and collection properties, such as surface recombination, carrier concentration, and minority carrier lifetime. These reports are interesting in comparison with recent reports of single-nanowire Si solar devices based on coaxial junctions.[14]

Vertically oriented Si nanowires were grown on intrinsic Si (111) substrates by a Au-catalyzed, VLS chemical vapor deposition process.[15] To produce the catalyst islands necessary for nanowire growth, a 100 nm Au film was first thermally evaporated onto the substrate, then annealed at 1050 °C for 20 min under 1 atm of H_2 at a flow rate of 1000 standard cm^3 per min (sccm). Si nanowires were then grown at this temperature and pressure by introducing $SiCl_4$ gas (Strem, 99.9999%) for 20 min at a flowrate of 20 sccm, while continuing the flow of H_2 at 1000 sccm. This process produced hexagonally faceted Si wires with diameters from 30 nm to 30 μm and lengths of over 50 μm, as observed in scanning electron microscopy (SEM) images.[16] Sawtooth faceting[17] was also observed on the sidewalls of the nanowires. Transmission electron microscopy has shown that Si wires grown under similar conditions in our reactor are single-crystalline and grow in the ⟨111⟩ direction.[11]

Four-probe electrical contacts to individual nanowires were fabricated using a procedure of photolithography, metallization, and lift-off. The nanowires were first removed from the growth substrate by sonication in isopropanol. This solution of suspended nanowires was deposited onto degenerately doped n-type Si wafers coated with 100 nm of Si_3N_4 and allowed to dry. This process yielded sparsely scattered

* Corresponding authors. E-mails: (N.S.L.) nslewis@caltech.edu; (H.A.A.) haa@caltech.edu.

10.1021/nl072622p CCC: $40.75 © 2008 American Chemical Society
Published on Web 02/13/2008

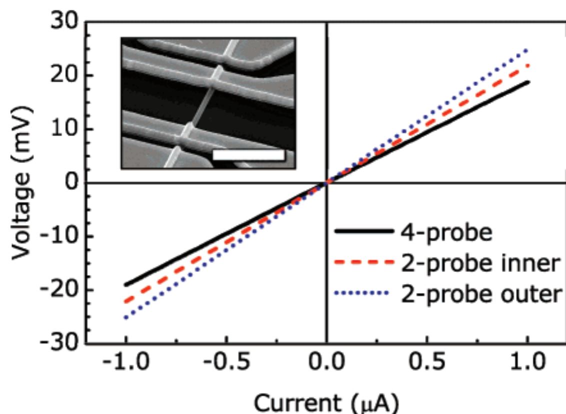

Figure 1. *I−V* analysis of a representative Si nanowire, showing ohmic behavior. Inset: 45° view SEM image of the wire and the 4-probe Al/Ag contacts. The scale bar on the inset is 10 μm.

nanowires lying flat on the substrate surface. The nanowire-covered substrates were then coated with photoresist films.[18] Contact patterns were aligned to individual nanowires and exposed using a conventional optical mask aligner. After development of the resist, the samples were immersed in buffered HF(aq) for 20 s to remove the native oxide from the exposed portions of the nanowires. The contacts were deposited by thermal evaporation of 300 nm of Al, which was chosen for its ability to form an ohmic contact to Si and to act as a p-type dopant. Ag (900 nm) was added on top of the Al to supplement the film thickness and to fully cover the larger-diameter wires. Lift-off was performed by immersion in photoresist remover for 30 min at 60 °C. The above procedure is a high-yield, single-lithographic step method for contacting semiconductor nano- and microwires ranging in diameter from 200 nm to 1.5 μm. Wires smaller than 200 nm in diameter could not be imaged in the optical mask aligner, and wires larger than 1.5 μm required metal films that were too thick for lift-off.

Two-, three-, and four-probe *I−V* measurements were performed to characterize each contact and each nanowire device. All of the devices had the same probe geometry with an inner probe spacing of 10 μm, and all figures henceforth correspond to a representative device with a 900 nm diameter. As shown in Figure 1, the as-deposited contacts generally showed ohmic behavior with contact resistances on the order of wire resistances. Back-gated measurements[19] revealed that the as-grown nanowires exhibited n-type behavior. The effective resistivity and doping level of the nanowires were calculated based on the observed resistance and the measured dimensions, assuming uniform current transport with bulk silicon carrier mobilities.[20] These effective bulk resistivities ranged from 0.02 to 0.08 Ω cm, which correspond to electrically active dopant concentrations of 1×10^{18} to 1×10^{17} cm^{-3}, respectively.

Rectifying junctions were selectively introduced beneath a single contact by electrically heating a segment of the nanowire. Such nanoscale joule heating has recently been employed for selective surface functionalization of Si nanowires.[21] In our process, the current was slowly increased between adjacent outer contacts until the enclosed nanowire segment was destroyed due to an extreme current density, typically >10 kA cm^{-2} (Figure 2a inset). In some cases, this produced a rectifying junction beneath the inner contact to the remaining portion of the nanowire, which exhibited photovoltaic behavior. While the nature of the induced junction is not explicitly understood, we believe that the observed rectifying behavior is likely due to the formation of a Schottky barrier, a p-n alloy junction, or a combination of these effects. There are several possible explanations for how such junctions could be formed. Al contacts to planar Si have been used previously to fabricate photovoltaic devices, either as Schottky junctions[22,23] or as aluminum alloy p-n junction diodes.[24] Schottky photovoltaic devices are possible because annealed Al−Si contacts can exhibit Schottky barrier heights of up to 0.8 V with increasing heat treatment temperatures.[25,26] At temperatures above the Al−Si eutectic point (577 °C), a p-n aluminum alloy junction solar cell can be formed in n-type silicon, because after cooling Al acts as a p-type dopant in the recrystallized Si.[27] Regardless of the nature of the junction, excellent rectification behavior was obtained (Figure 2a).

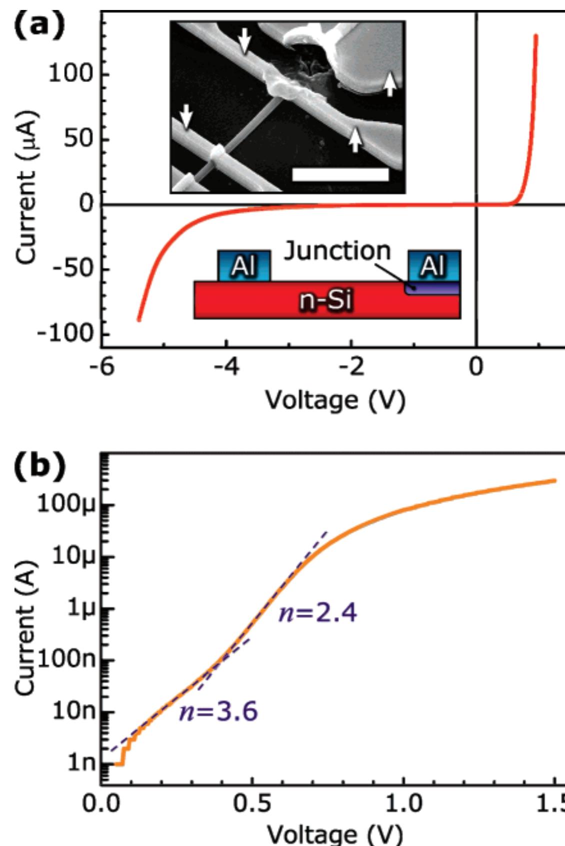

Figure 2. (a) Dark *I−V* measurement of a single, 900 nm diameter Si nanowire diode device. Inset: 45° view SEM image. The scale bar is 10 μm. The rectifying junction was formed by sourcing current between the adjacent upper contacts (upward-facing arrows) until the enclosed wire segment was destroyed. The *I−V* data were then measured between the two inner contacts (downward-facing arrows). (b) Log scale plot of the forward bias dark *I−V* data with linear fits illustrating the extracted diode ideality factor, *n*.

The dark *I−V* characteristics of the Si nanowire photovoltaic devices were measured, as shown in Figure 2a,b. The forward bias dark *I−V* data showed ideality factors, *n*,

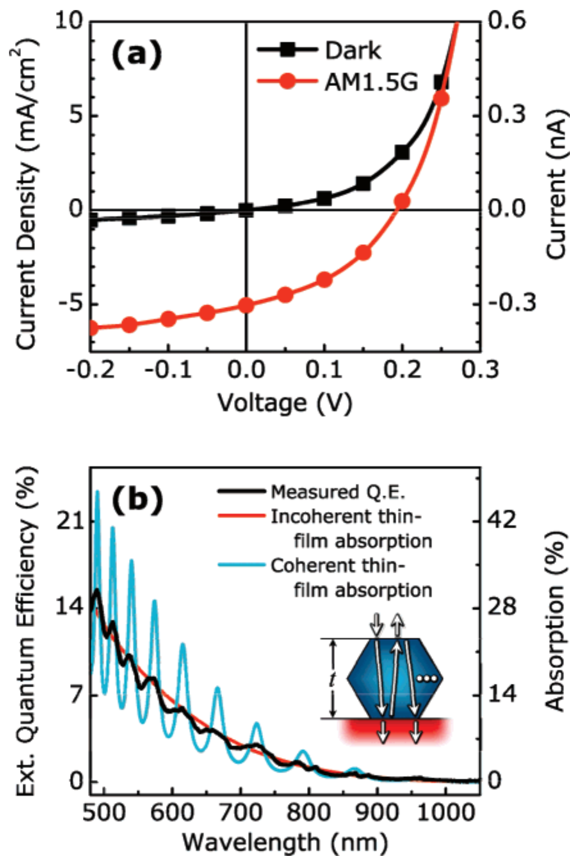

Figure 3. Photovoltaic performance of a single Si nanowire solar cell with a 900 nm diameter ($t = 780$ nm). (a) Dark/light $J-V$ data with the current density normalized to the light absorption cross-sectional area (left axis.) The device current magnitude is plotted on the right axis. (b) Spectral response data showing the external quantum efficiency of the same nanowire device. The calculated absorbance for a thin silicon film of the same thickness, t, under assumptions of incoherent and coherent interference at the front and back surface is shown for comparison.

ranging from 2.0 to 3.6. Typical devices showed an ideality factor of ~3.5 for biases from 0.15 to 0.3 V, and an ideality factor of ~2.5 for biases from 0.4 to 0.6 V (Figure 2b.) These values are consistent with the ideality factors reported for Al–Si photovoltaic Schottky junctions.[22] The series resistance observed at high forward biases (>1 V) was approximately equal to the wire resistance plus the contact resistance measured prior to junction formation. Reverse breakdown occurred between −5 and −10 V (Figure 2a), which is near the expected threshold for avalanche or tunnel breakdown for a one-sided abrupt junction at the estimated doping levels of our devices.[20]

Upon illumination, these single-junction Si nanowire devices exhibited clear photovoltaic behavior. Figure 3a shows a current density–voltage ($J-V$) measurement of a single-nanowire solar cell under AM 1.5G illumination. The measured current has been normalized to the light collection (top-down) area of the nanowire rather than the cross-sectional area of the nanowire. This cell exhibited an open-circuit voltage, V_{oc}, of 190 mV, a short-circuit current density, J_{sc}, of 5.0 mA cm^{-2}, and a fill factor of 0.40, which corresponds to an overall solar energy conversion efficiency of 0.46%.

The spectral response of the solar cell is shown in Figure 3b. These data were obtained using a supercontinuum laser source (Fianium) and a monochromator with an average passband of 1 nm. No additional focusing optics were employed. This source yielded a spot (>1 mm^2 in area) of uniform illumination, whose spectral power density (W m^{-2} nm^{-1}) ranged from 1 to 5 suns (AM 0) throughout the measurement range. The observed external quantum efficiency can be explained by thin-film absorption with partially coherent interference effects. SEM imaging[28] confirmed that the wire was hexagonally faceted with the front (top) and back (bottom) facets oriented normal to the direction of illumination, as illustrated in Figure 3b (inset). The wire thus formed a thin-film absorber layer with a well-defined thickness equal to the minor chord of the hexagonal cross-section of the wire, defined as dimension t in Figure 3b (inset). On the basis of published values of the absorption and refractive index of Si,[29] the expected absorbance of a thin film of thickness t can be calculated for the cases of coherent and incoherent interference, respectively, at the front and back surfaces (Figure 3b.) The excellent agreement between the peak locations for coherent thin-film absorption and the measured quantum efficiency indicate that there is likely interference at the front and back surfaces of the nanowire. However, the limited magnitude of the peaks reveals that the interference is partial, limited perhaps by the wire surface roughness, which was easily observed as sawtooth faceting in SEM images, or by the effects of the other nanowire facets, which were ignored in the calculation. The overall agreement between the expected thin-film absorption and our measured external quantum efficiency also indicates that the internal quantum efficiency was fairly constant across all measured wavelengths. This is expected because carriers must diffuse roughly the same distance to the junction regardless of whether they are excited nearer the top facet or the bottom facet of the nanowire. Such orthogonalization of carrier absorption and collection in Si solar cells has been proposed to obtain high quantum efficiency across all energies of illumination above the Si band gap, for example, in radial junction nanowire cells[10] and in vertical multijunction[30,31] solar cells.

Scanning photocurrent microscopy (SPCM) was performed using a confocal microscope and a near-field scanning optical microscope (NSOM) tip to map the local photocarrier collection within our nanowire devices. This technique has been used by others to study the band structure,[32] contact effects,[13] and carrier transport[33,34] of nanowires, as well as to determine the minority carrier diffusion length in CdS devices similar to the Si nanowire solar cell described herein.[12] For SPCM measurements, a semiconductor diode laser provided 650 nm optical excitation, which was modulated at 2 kHz. The beam was then focused to a spot size of ~1.0 μm through the 60× objective of a confocal microscope (WiTEC AlphaSNOM.) For near-field excitation, this beam was then sent through the tip of a cantilevered contact-mode NSOM probe with an optical aperture of 500 nm. The photocurrent was recorded as a function of the tip position and device bias using a current preamplifier[35] and lock-in

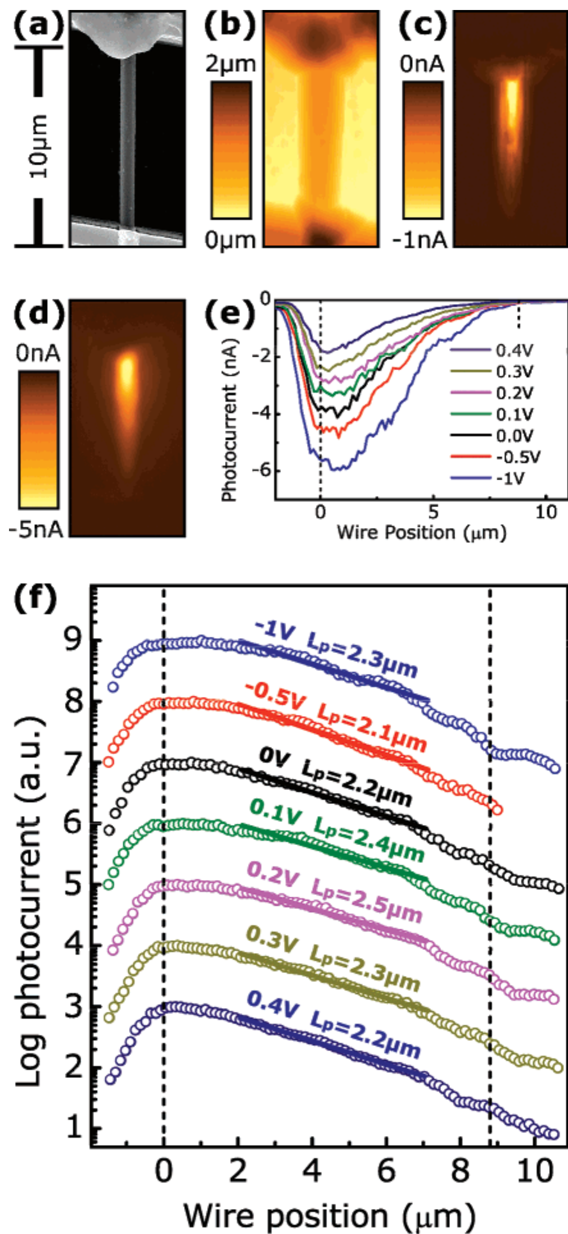

Figure 4. SPCM measurements of a single Si nanowire solar cell with a 900 nm diameter. The scale bar applies to images (a−d). (a) SEM image, (b) NSOM topography map, (c) NSOM SPCM image at −1 V bias, (d) confocal SPCM image at −1 V bias, (e) line scans of confocal SPCM measurements obtained for several biases, and (f) log-scale line scans of photocurrent as a function of the illumination position along the wire. The exponential fits enable extraction of the minority carrier (hole) diffusion length, L_p. The scans have been offset for clarity. In panels e and f, the dashed vertical lines indicate the length of the wire with the junction located at 0 μm.

detection. An SEM image of a representative nanowire device is presented in Figure 4a. The topography and photocurrent map of this device were recorded using a NSOM tip and are shown in Figure 4b,c, respectively. Finally, the NSOM tip was removed and a confocal-mode photocurrent image was obtained (Figure 4d). Use of the NSOM tip provided greater spatial resolution than confocal microscopy, but the NSOM images were influenced by the presence of small metal particles on the nanowire surface due to the partial melting the Al/Ag contact during junction formation. The overall agreement between the photocurrent profiles obtained with NSOM and confocal-mode SPCM methods indicates that confocal illumination was adequate to study the carrier collection in our nanowires despite its lower spatial resolution.

The SPCM images were analyzed to determine the charge collection properties of the Si nanowire devices. Negative photocarrier collection was observed with a peak nearest the rectifying junction (Figure 4e). The collected current decayed exponentially away from the junction at both reverse and forward biases, and the exponential decay rate of the photocurrent did not change with the bias. This behavior is consistent with minority carrier diffusion-limited carrier transport within the quasi-neutral region of the nanowire solar cell with negligible drift current contribution. In this situation, exponential fits to line scans from confocal-mode SPCM measurements (Figure 4f) allow the direct extraction of minority carrier diffusion lengths within the n-type base of the nanowire solar cell. Hole diffusion lengths, L_p, ranged from 2 to 4 μm for the devices measured.

By assuming that the observed hole diffusion length is limited solely by bulk recombination, one can obtain a lower limit of the nanowire bulk hole lifetime. Using values for the mobility identical to that of bulk Si[20] at the measured doping density ($N_D = 10^{18}$ cm^{-3}), the hole lifetime, τ_p, is calculated as ~15 ns ($\tau_p = L_p^2/D_p$, with $D_p = kT/q\mu_p$ as the hole diffusion coefficient). This value is larger than expected but reasonable in comparison with the predicted bulk carrier lifetimes for Si doped with Au at its solid solubility limit at our VLS growth temperature of 1050 °C. At this temperature, Au can diffuse into Si up to concentrations of 10^{16} atoms cm^{-3}, producing expected minority hole lifetimes from 2 to 4 ns.[36] However, it is not clear that such gold concentrations would be obtained in VLS nanowires as, for example, growth of single-crystalline Si from a melt tends to limit Au incorporation to 10^{15} atoms cm^{-3}.[36] This effect could lead to lower bulk Au concentrations than predicted by the solid solubility alone, which in turn could lead to a slightly higher bulk carrier lifetime.

Alternatively, by assuming that the effective hole lifetime is limited solely by surface recombination, one can obtain an upper limit on the surface recombination velocity. This calculation is performed by solving the charge-transport equation in radial coordinates for a cylindrical wire of diameter equal to the thickness of the measured wire (t) in the absence of bulk recombination. The surface recombination velocity, S, was varied to obtain an excess carrier decay rate throughout the wire equivalent to a bulk recombination lifetime of 15 ns. In this case, we calculate a maximum surface recombination velocity of approximately 1350 cm sec^{-1}, which is reasonable for a native oxide on (111)-oriented n-type Si.[37] Further experiments will be needed to separately elucidate the bulk and surface minority carrier recombination rates. However, if the carrier lifetimes are indeed limited by surface recombination, surface passivation efforts have the potential to increase the effective minority carrier diffusion lengths beyond those measured in this study.

In conclusion, a simple method has been developed for creating rectifying contacts that yield photovoltaic behavior from single silicon nanowires. These devices can be used to gain insight into the performance-determining properties for nanowire photovoltaics, such as the resistivity and diffusion length, as well as the rates of bulk and surface recombination. Because of the hexagonal faceting of the wires studied, interference led to some chromatic absorption enhancements. This behavior suggests that the geometry of nanowire devices can be manipulated to optimize the optical absorption or transmission at selected wavelengths. We have also observed diffusion lengths of $>2\ \mu$m in gold-catalyzed, VLS-grown, silicon nanowires, which is to our knowledge the longest diffusion length reported to date in single semiconductor nanowires. In radial junction devices, the tradeoff between small-diameter wires (which favor greater current collection) and larger-diameter wires (which yield higher photovoltages due to decreased junction area) is optimized when the wire radius is approximately equal to the minority carrier diffusion length.[10] Thus, for these particular growth methods and conditions, we conclude that future efforts toward the development of this cell should target wires of $\geq 4\ \mu$m in diameter.

Acknowledgment. This work was supported by BP and in part by the National Science Foundation under Grant DMR 0606472 and also made use of facilities supported by the Center for Science and Engineering of Materials, an NSF Materials Research Science and Engineering Center at Caltech.

Supporting Information Available: SEM image of as-grown nanowires, SEM images of contacted nanowire devices showing faceting, and circuit schematic of SPCM preamplifier. This material is available free of charge via the Internet at http://pubs.acs.org.

References

(1) Tsakalakos, L.; Balch, J.; Fronheiser, J.; Shih, M. Y.; Leboeuf, S. F.; Pietrzykowski, M.; Codella, P. J.; Korevaar, B. A.; Sulima, O. V.; Rand, J.; Davulura, A.; Rapol, U. *J. Nanophoton.* **2007**, *1*, 013552−10.

(2) Peng, K.; Xu, Y.; Wu, Y.; Yan, Y.; Lee, S.-T.; Zhu, J. *Small* **2005**, *1*, 1062−1067.

(3) Hu, L.; Chen, G. *Nano Lett.* **2007**, *7*, 3249−3252.

(4) Huynh, W. U.; Dittmer, J. J.; Alivisatos, A. P. *Science* **2002**, *295*, 2425−2427.

(5) Law, M.; Greene, L. E.; Johnson, J. C.; Saykally, R.; Yang, P. D. *Nat. Mater.* **2005**, *4*, 455−459.

(6) Baxter, J. B.; Aydil, E. S. *Appl. Phys. Lett.* **2005**, 86.

(7) Leschkies, K. S.; Divakar, R.; Basu, J.; Enache-Pommer, E.; Boercker, J. E.; Carter, C. B.; Kortshagen, U. R.; Norris, D. J.; Aydil, E. S. *Nano Lett.* **2007**, *7*, 1793−8.

(8) Maiolo, J. R. I.; Kayes, B. M.; Filler, M. A.; Putnam, M. C.; Kelzenberg, M. D.; Brunschwig, B. S.; Atwater, H. A.; Lewis, N. S. *J. Am. Chem. Soc.* **2007**, *129*, 12346−12347.

(9) Goodey, A. P.; Eichfeld, S. M.; Lew, K.-K.; Redwing, J. M.; Mallouk, T. E. *J. Am. Chem. Soc.* **2007**, *129*, 12344−12345.

(10) Kayes, B. M.; Atwater, H. A.; Lewis, N. S. *J. Appl. Phys.* **2005**, *97*, 114302−11.

(11) Kayes, B. M.; Filler, M. A.; Putnam, M. C.; Kelzenberg, M. D.; Lewis, N. S.; Atwater, H. A. *Appl. Phys. Lett.* **2007**, *91*, 103110−3.

(12) Allen, J. E.; Yi, G.; Romankiewicz, J. P.; Lensch, J. L.; May, S. J.; Odom, T. W.; Wessels, B. W.; Lauhon, L. J. In *Measurement of Minority Carrier Diffusion Lengths in Semiconductor Nanowires*; IEEE Device Research Conference, University Park PA; IEEE: Piscataway, NJ, 2006; pp 289−290.

(13) Gu, Y.; Romankiewicz, J. P.; David, J. K.; Lensch, J. L.; Lauhon, L. J.; Kwak, E. S.; Odom, T. W. *J. Vac. Sci. Technol., B* **2006**, *24*, 2172−2177.

(14) Tian, B.; Zheng, X.; Kempa, T. J.; Fang, Y.; Yu, N.; Yu, G.; Huang, J. Lieber, C. M. *Nature* **2007**, *449*, 885−889.

(15) Wagner, R. S.; Ellis, W. C. *Appl. Phys. Lett.* **1964**, *4*, 89−90.

(16) A SEM image of the as-grown nanowires appears in the Supporting Information for this publication.

(17) Ross, F. M.; Tersoff, J.; Reuter, M. C. *Phys. Rev. Lett.* **2005**, *95*, 146104−4.

(18) The greatest device yield was obtained using two layers of LOR3A (Microchem) spun at 1300 RPM and baked at 190 °C, followed by a single layer of S1813 (Microchem) spun at 3000 RPM and baked at 115 °C. Lift-off was performed using Remover PG (Microchem) at 60 °C for 30 min. Caution was taken with this combustible liquid, as the flash point is 88 °C.

(19) See, for example, Cui, Y.; Zhong, Z. H.; Wang, D. L.; Wang, W. U.; Lieber, C. M. *Nano Lett.* **2003**, *3*, 149−152.

(20) Sze, S. M.; Kwok, K. N. *Physics of Semiconductor Devices*; John Wiley & Sons: Hoboken, NJ, 2007.

(21) Park, I.; Li, Z.; Pisano, A. P.; Williams, R. S. *Nano Lett.* **2007**, *7*, 3106−3111.

(22) Thomson, D. J.; Matiowsky, M. A.; Card, H. C. *Electron. Lett.* **1981**, *17*, 382−383.

(23) Thomson, D. J.; Mejia, S.; Card, H. C. *J. Power Sources* **1982**, *7*, 191−194.

(24) Meier, D. L.; Davis, H. P.; Garcia, R. A.; Salami, J.; Rohatgi, A.; Ebong, A.; Doshi, P. *Sol. Energy Mater. Sol. Cells* **2001**, *65*, 621−627.

(25) Card, H. C. *IEEE Trans. Electron Devices* **1976**, *23*, 538−544.

(26) Chino, K. *Electr. Commun. Lab. Tech. J.* **1972**, *21*, 1765−1780.

(27) Gudmundsen, R. A. *J. Appl. Phys.* **1957**, *28*, 1308−1316.

(28) SEM images showing nanowire faceting appear in the Supporting Information for this publication.

(29) Aspens, D. E., Optical Properties of Si. In *Properties of Crystalline Silicon*; Hull, R., Ed.; INSPEC, IEE: London, 1999; p 677.

(30) Chadda, T. B. S.; Wolf, M. In *Comparison of Vertical Multi-Junction and Conventional Solar Cell Performance*; IEEE: New York, 1974; pp 52−57.

(31) Rahilly, W. P. In *Vertical Multijunction Solar Cells*; Record of the Ninth IEEE Photovoltaic Specialists Conference, Silver Spring, MD; IEEE: New York, 1972; pp 44−52.

(32) Yeonghwan, A.; Dunning, J.; Park, J. *Nano Lett.* **2005**, *5*, 1367−1370.

(33) Gu, Y.; Romankiewicz, J. P.; Lauhon, L. J. In *Quantitative Characterization of Carrier Transport in Nanowire Photodetectors*; Proceedings of SPIE, 2007; Vol. 6479, 64790C.

(34) Gu, Y.; Romankiewicz, J. P.; David, J. K.; Lensch, J. L.; Lauhon, L. J. *Nano Lett.* **2006**, *6*, 948−952.

(35) A circuit schematic of the current preamplifier appears in the Supporting Information for this publication.

(36) Bullis, W. M. *Solid-State Electron.* **1966**, *9*, 143−168.

(37) Michalak, D. J.; Lewis, N. S. *Appl. Phys. Lett.* **2002**, *80*, 4458−4460.

NL072622P